Heliyon 6 (2020) e03868

Contents lists available at ScienceDirect

Heliyon

journal homepage: www.cell.com/heliyon

Research article

Fe(III)-polyhydroxy cations supported onto K10 montmorillonite for removal of phosphate from waters

Samara T. Leite, Fernando H. do Nascimento, Jorge C. Masini *

Departamento de Química Fundamental, Instituto de Química, Universidade de São Paulo, 05508-000, São Paulo, SP, Brazil

ARTICLE INFO

Keywords:
Environmental science
Materials chemistry
Phosphate
Montmorillonite
Fe^{3+} polyhydroxy cations
Adsorption
Waters
Eutrophication

ABSTRACT

Since phosphate is strongly related to eutrophication of environmental waters, several research groups quest for materials that can efficiently remove phosphate from wastewaters before it contaminates lakes and reservoirs. In the present work, a commercial clay mineral (K10 montmorillonite) modified with Fe^{3+} polyhydroxy cations was investigated as an adsorbent for phosphate. The incorporation of the polycations did not alter the main conformational characteristics of the montmorillonite, as verified by specific surface area measurements, X-ray diffractometry, FTIR, electron microscopy, and zeta potential titrations. On the other hand, the materials supporting Fe^{3+} polyhydroxy cations exhibited a significant enhancement of adsorption capacity, as determined by Langmuir-Freundlich isotherms, from 39 ± 2 to 104 ± 15 μmol g^{-1}. The different ratios of OH^- to Fe^{3+} did not affect the adsorption capacities. The adsorption kinetics was best described by the pseudo 2nd order model, approaching the equilibrium after 120 min of contact time. A variation of pH between 4.6 and 8.5 did not affect the adsorption percentages. The adsorption capacities increased with the increase of the ionic strength, thus suggesting that the formation of inner-sphere complexes prevails over electrostatic interactions as the adsorption mechanism. The materials removed phosphate from three polluted water samples having phosphate concentrations between 0.0919 and 1.211 mg L^{-1}. The remaining phosphate concentration was below the limit of quantification of the analytical method (0.063 mg L^{-1} in P, or 2.0 μmol L^{-1}). The presence of 10 mg L^{-1} humic of fulvic acid did not affect the performance of the materials. In conclusion, the modification of clay minerals with Fe^{3+} polyhydroxy cations is useful in producing low-cost adsorbents for phosphate.

1. Introduction

High availability of phosphate causes the eutrophication and uncontrolled growth of cyanobacteria in aquatic environments. These microorganisms may release potent toxins that remain in the waters after conventional treatment (Cunha et al., 2017). Strategies for removal of phosphate include chemical precipitation, biological treatment, ion exchange, tertiary filtration, and adsorption (Tian et al., 2009). Adsorption is among the most efficient technologies because it relies on low-cost materials such as aluminum and iron oxides or oxyhydroxides, zeolites, clay minerals, silicates, etc. Since adsorption is not a destructive technique, some materials release the nutrient after the treatment, thus attending the demands of a circular economy (Kasprzyk and Gajewska, 2019). Recent research has proposed a variety of adsorbents including layered chalcogenide (Li et al., 2019), nano-porous calcined palygorskite embedded with $La(OH)_3$ (Kong et al., 2018), acid-activated akadama clay (a Japanese volcanic soil) (Wang et al., 2018), magnetically recoverable magnetite/lanthanum hydroxide (Fang et al., 2018), hydrothermally synthesized lanthanum carbonate nanorods (Koh et al., 2020), thermally activated dolomite (Ivanets et al., 2015, 2016), zirconium/magnesium modified bentonite (Lin et al., 2020), etc.

Clay minerals have gained interest because they are abundant in nature and are environmentally compatible. Montmorillonites, like other smectites, have permanent negative charges generated by the isomorphic substitutions of Si^{4+} by Al^{3+} in the tetrahedral sheets, and of Al^{3+} by Mg^{2+} in the octahedrons. Exchangeable cations such as Na^+, Ca^{2+}, and Mg^{2+} in the interlayer counterbalance these negative charges. The interlayer cations can be exchanged by Al^{3+}, Fe^{3+}, Ti^{4+}, Cr^{3+}, Zr^{4+}, known to form polynuclear cationic species under hydrolysis, thus increasing the affinity of these materials towards adsorption of oxyanions (Mdlalose et al., 2019). Additionally, the reactivity of the surface silanol and aluminol groups enables easy chemical modifications to enhance their affinity towards different pollutants (Abate and Masini, 2005a; do Nascimento et al., 2016; Uddin, 2017; Adewuyi and Oderinde, 2019).

* Corresponding author.
E-mail address: jcmasini@iq.usp.br (J.C. Masini).

https://doi.org/10.1016/j.heliyon.2020.e03868
Received 20 December 2019; Received in revised form 18 March 2020; Accepted 23 April 2020

Modification of bentonites (a mixture of clay minerals containing 60–80% montmorillonite) with La^{3+} has been the basis for producing commercially available sorbents for phosphate, namely the Phoslock® product. The uptake of phosphate occurs by the formation of $LaPO_4$, which precipitates on the surface of the clay support. Neither La^{3+} nor PO_4^{3-} is released in a wide range of pH (Zamparas et al., 2015; de Castro et al., 2018).

The widespread occurrence of phosphate in water bodies has motivated the quest for efficient and low-cost adsorbents based on clay minerals (Funes et al., 2018). Tian et al. (2009) investigated the use of bentonite pillared with Al^{3+} and mixtures of Al^{3+} and La^{3+} polyhydroxy cations, finding that the mixed systems provided higher adsorption capacities. de Castro et al. (2018) investigated the intercalation of two montmorillonites with mixtures of La^{3+} and Fe^{3+}, stating that the use of Fe^{3+} is economically advantageous since Fe^{3+} salts are less expensive than La^{3+} ones. However, modification with La^{3+} renders materials that are not susceptible to redox reactions.

Shanableh et al. (2016) demonstrated the better performance of bentonites modified with mixed trivalent cations over the materials modified with a single cation. In this case, the authors intercalated a bentonite sample with Fe^{3+}, Al^{3+}, and mixed Fe^{3+} and Al^{3+} polyhydroxy cations. This behavior is not a general rule, and the performance of the materials seems to depend on the starting bentonite and the modification procedure. Yan et al. (2010), for instance, found the following order of adsorption capacities for pillared bentonites: OH^--Al^{3+} > OH^--Fe^{3+} > mixed OH^--Fe^{3+}/Al^{3+}. Zirconium-containing adsorbents have gained considerable attention because hydrous zirconium oxide is non-toxic, environmentally friendly, not dissolvable in water, and interacts with phosphate via ligand exchange and inner-sphere complex formation (Huang et al., 2015; Lin et al., 2018, 2020).

Iron species are environmentally friend modifiers of clay minerals. Iron oxy-hydroxides occur naturally in either the interlamellar space or covering the surface of clay particles in soils and sediments (Savic et al., 2012). Exploring this natural phenomenon, Borgnino et al. (2009) synthesized Fe^{3+} montmorillonites for phosphate adsorption, finding that the modified materials exhibited enhanced adsorption capacity over their unmodified counterparts. Fe^{3+} modified Zenith bentonite followed a similar pattern (Zamparas et al., 2012).

In the present work, the commercial K10 Mt was modified with Fe^{3+} polyhydroxy cations obtained by mixing OH^- and Fe^{3+} at the stoichiometric ratios of 0.75: 1, 1:1, and 2:1. Compared with the K10 Mt, the modified materials exhibited enhanced affinity and adsorption capacity towards phosphate. The pH affected only slightly the adsorption in the typical pH range of natural waters. The increase of ionic strength enhanced the adsorption. Humic and fulvic acid did not affect the adsorption, suggesting the materials have potential applicability to remove phosphate from natural and polluted waters.

2. Experimental

2.1. Materials

The K10 Mt was purchased from Aldrich and used as received. This material has a cation exchange capacity of 0.59 ± 0.01 mmol g^{-1} and a BET specific surface area of 228 m^2 g^{-1} (Abate and Masini, 2005b). Analytical grade $FeCl_3$, NaOH, KH_2PO_4, K_2HPO_4, sodium salt of humic acid, $NaNO_3$, $NaNO_2$, and NH_4Cl were from the Merck Group. Fulvic acid was isolated from vermicompost as described elsewhere (Abate et al., 2006).

2.2. Preparation of the Fe(III) polycations and modification of Mt

Under vigorous stirring, adequate volumes of 1.0 mol L^{-1} NaOH solution were pumped (1.0 mL min^{-1}) to 250.0 mL of 0.40 mol L^{-1} $FeCl_3$ to produce 0.75:1, 1:1 or 2:1 [OH^-]: [Fe^{3+}] molar ratios. The obtained suspensions were heated at 50 °C for 48 h under continuous agitation at 250 r.p.m. in a thermostated orbital shaker form Marconi (Piracicaba, SP, Brazil). Next, dispersions containing 10.0 g of Mt were heated at 50 °C, and the suspensions of the Fe^{3+} polyhydroxy cations were added at a flow rate of 1.0 mL min^{-1} under vigorous stirring, providing a ratio of 10 mmol of Fe^{3+} per gram of Mt. The dispersions were left standing for 72 h.

The dispersions were centrifuged at 4000 × *g* for 30 min in a Sorvall ST16R centrifuge (Thermo Fisher Scientific, Waltham, MA, USA), and the solid phases were washed five times with deionized water, always separating the solid by centrifugation. The modified Mt was dried in an oven at 100 °C for 24 h, disintegrated in a ceramic mortar and pestle, and stored in a desiccator. The materials prepared with [OH^-]: [Fe^{3+}] molar ratios 0.75:1, 1:1, and 2:1 were identified as Mt-OH/$Fe_{0.75:1}$, Mt-OH/$Fe_{1:1}$, and Mt-OH/$Fe_{2:1}$, respectively.

The specific surface area was obtained from BET measurements of N_2 adsorption isotherms using a Gemini 2375 V5.00 instrument from Micromeritics Instr. Corp. The pore volume was determined at P/P_0 ratio of 0.95, while the micropore volumes were determined by the t-plot method. The basal spacing of Mt and Fe^{3+}-intercalated Mt was estimated by X-Ray diffraction (XRD) using a Siemens D-5000 diffractometer. Electron microscopy (SEM and TEM) was made with a Fesem Jeol JSM -740 1 F instrument (Jeol Ltda, Tokyo, Japan). For TEM analyses, the samples were supported in Cu-made 3-mm grids.

For quantification of the iron contents of the starting and modified Mt, 30 mg of the samples were extracted with 2.50 mL of 2.0 mol L^{-1} HCl for three hours, followed by centrifugation to separate the supernatant phase. After three extractions, the supernatant phases were mixed and analyzed by flow injection analysis with spectrophotometric detection of the $Fe(SCN)_6^{3-}$ complex at 480 nm.

2.3. Adsorption experiments

Batch adsorption/desorption experiments were made in the thermostatic orbital shaker at the stirring rate of 250 r.p.m., and 25.0 ± 0.5 °C. All the adsorption/desorption experiments were done in polypropylene centrifuge tubes from Corning® (capacity of 15 mL), horizontally accommodated inside the shaker. Dispersions were centrifuged at 4,000 × g for 15 min and filtered through 0.45-μm syringe filters (hydrophilic Minisart®, Sartorius Stedim Biotech GmbH, Germany).

The effect of dose and contact time was investigated by adsorption experiments made with 25.0, 50.0, 75.0, and 100 mg of adsorbent dispersed in 10.0 mL of 3.23 × 10^2 μmol L^{-1} phosphate buffer (pH 6.9) (10 mg L^{-1} in P). The contact times were up to 240 min.

Adsorption isotherms were constructed by adopting 180 min of contact time, using 100 mg of adsorbent dispersed in 10.0 mL of phosphate solutions (pH 6.9). The temperature was 25.0 ± 0.5 °C and the initial concentrations were between 3.23 × 10^2 and 3.23 × 10^3 μmol L^{-1} (10–100 mg L^{-1} in P). The dispersions were centrifuged at 4,000 × g, and the supernatants were carefully separated, avoiding resuspension of the centrifuged adsorbent. The supernatants were filtered through syringe filters and stored in the refrigerator (4 °C) until the moment of analysis. For the desorption experiments, 10.0 mL of deionized water was added to the centrifuge tubes containing the adsorbent, and the tubes were vortexed to disperse the pellets and then agitated in the orbital shaker at 250 r.p.m. for 180 min at 25.0 ± 0.5 °C. After this, the dispersions were centrifuged, and the supernatants were filtered and analyzed as described for the adsorption studies. For determination of the hysteresis, the tube containing initially 100 mg of adsorbent and 10.0 mL of a 645.7 μmol L^{-1} phosphate solution (20.0 mg L^{-1} in P) was extracted with three aliquots of deionized water (10.0 mL), each extraction lasting 180 min in the horizontal shaker at 25.0 ± 0.5 °C.

Spectrophotometric determination of the free phosphate concentrations was based on the reaction with ammonium molybdenum (2.5 × 10^{-3} mol L^{-1} in 0.20 mol L^{-1} HNO_3) followed by the reduction of Mo(VI) to Mo(V) by 5.0% (m v^{-1}) ascorbic acid in the presence of 100 mg L^{-1} Sb as catalyst (Galhardo and Masini, 2000). Absorbance measurements were made in an Ocean Optics USB4000 spectrometer and an LS-1-LL

tungsten-halogen light source, both connected by two-optical fibers (600 μm diameter, 1 m long) to a 1-cm pathlength flow cell.

2.4. Samples

Two samples from the Billings reservoir (BR1 and BR2) and one sample from the Pinheiros river (PR1), both located in the metropolitan area of São Paulo city, São Paulo, Brazil, were provided by the São Paulo State Environmental Company (CETESB). The adsorption experiments were made using 50.0 mg of adsorbent dispersed in 5.0 mL of the sample before and after enrichment with 2.50 mg P L^{-1} (80.7 μmol L^{-1}).

2.5. Data treatment

The adsorbed amount of phosphate (q) was computed as:

$$q = \frac{(C_{P,i} - C_P)V}{m} \quad (1)$$

where $c_{P,i}$ is the initial concentration of phosphate (in μmol L^{-1}), c_P is the free concentration after a given contact time with the adsorbent, V is the volume of solution where the adsorbents were dispersed (10.0 mL), and m is the mass of adsorbent.

2.5.1. Adsorption kinetics

The experimental data were fitted by the Lagergren's first order, pseudo 2nd order, and intraparticle diffusion kinetic models, given by Eqs. (2), (3), and (4), respectively:

$$q_t = q_e\left(1 - exp^{-k_1 t}\right) \quad (2)$$

$$q_t = \frac{q_e^2 k_2 t}{q_e k_2 t + 1} \quad (3)$$

$$q_t = k_{id} t^{0.5} + C \quad (4)$$

where q_t is the amount of phosphate (μmol) adsorbed per gram of adsorbent at time t, q_e is the fitted amount of phosphate adsorbed at the equilibrium (μmol g^{-1}), and k_1, k_2, and k_{id} are the Lagergren's 1st order, pseudo 2nd order, and intraparticle diffusion rate constants, respectively. The term C (Eq. (4)) is related to the thickness of the boundary layer.

2.5.2. Adsorption isotherms

The values of q plotted as a function of c_P were fitted to the Langmuir, Freundlich, and Langmuir-Freundlich equations (Eqs. (5), (7), and (9), respectively).

$$q = q_{max}\frac{K_L c_P}{1 + K_L c_P} \quad (5)$$

where q_{max} is the maximum amount of phosphate adsorbed per unit mass of soil (μmol g^{-1}), and K_L is the Langmuir adsorption constant (L μmol^{-1}).

From the K_L, it is possible to calculate the dimensionless constant separation factor (R_L) using Eq. (6):

$$R_L = \frac{1}{1 + K_L C_0} \quad (6)$$

Where C_0 is the largest initial concentration of adsorbate used in the adsorption isotherm (in μmol L^{-1}). If $0 < R_L < 1$, the adsorption is considered favorable, if $R_L > 1$ the adsorption is unfavorable and if $R_L = 0$ the adsorption is irreversible (Hall et al., 1966).

The Freundlich equation is represented by:

$$q = K_f c_P^{1/n} \quad (7)$$

where K_f is the Freundlich empirical constant related to adsorption capacity (μmol$^{1-1/n}$ g^{-1} $L^{1/n}$), and 1/n is the nonlinearity parameter associated with the energetic heterogeneity of the adsorption sites.

The hysteresis coefficient (H) for the adsorption/desorption was calculated by:

$$H = \frac{1/n_d}{1/n} \quad (8)$$

here, $1/n_d$ is the Freundlich nonlinearity parameter fitted from the sequential desorption isotherm.

The Langmuir-Freundlich model was tested:

$$q = q_{max}\frac{K_{LF} c_P^{n_2}}{1 + K_{LF} c_P^{n_2}} \quad (9)$$

where the K_{LF} is the adsorption affinity parameter, and n_2 refers to the Langmuir-Freundlich heterogeneity index.

All the fittings to Eqs. (2), (3), (5), (7), and (9) were made by non-linear regression analysis using the software Origin 8.0 (OriginLab Corp. Northampton, MA, USA).

3. Results and discussion

3.1. Characterizations

The X-ray diffractogram of the acid-activated K10 Mt exhibited a low-intensity reflection peak at 2θ = 5.74° (1.54 nm) (Figure 1), in agreement with diffractograms described for this material in other publications (dos Santos et al., 2015; Yang et al., 2015; Almasri et al., 2018). According to Wallis et al. (2007), this low intensity is a consequence of processes starting with the exchange of the interlayer cations by H^+, followed by delamination (producing disorientated aggregates), dissolution of the individual platelets, and formation of low crystallinity highly porous hydrous phase. High-intensity basal reflections indicate a large number of repeating clay platelets (Wallis et al., 2007) so that the used K10 Mt had a low degree of laminar stacking, which was further confirmed by SEM. Other reflections characteristic of Mt were observed at 2θ = 19.8° and 35° (Figure 1). Reflections related to muscovite (2θ = 8.9 and 17.9°), quartz (2θ = 20.9, 26.9 and 45.5°) and feldspar (2θ = 27.8°) (Figure 1) were also observed in agreement with other studies made with K10 Mt (Wallis et al., 2007; Kuźniarska-Biernacka et al., 2009; dos Anjos et al., 2014; dos Santos et al., 2015; Almasri et al., 2018). After modification

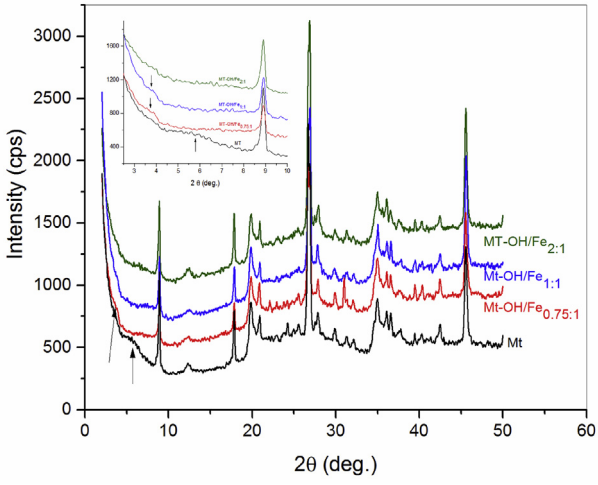

Figure 1. XRD patterns – Cu Kα - of the K10 Mt and Fe^{3+} polyhydroxy cations modified montmorillonite. The inset shows a zoom in the expected angles related do the d001 basal spacing.

with the Fe^{3+} polyhydroxy cations, the reflection at 5.74° (2θ) displaced to 4.0° (2θ), indicating an increase in the basal spacing of the remaining platelets, especially for Mt-OH/$Fe_{0.75:1}$ and Mt-OH/$Fe_{1:1}$. This increase is a consequence of the intercalation of the polyhydroxy cations in the interlayers of Mt. No reflections appeared for Mt-OH/$Fe_{2:1}$ in $2\theta < 8.9°$.

The specific surface area, obtained from BET measurements of N_2 adsorption isotherms, increased roughly 7–15% after the modification with the Fe^{3+} polyhydroxy cations, varying from 228 $m^2\ g^{-1}$ for Mt to about 246–270 $m^2\ g^{-1}$ in the modified materials. Similarly, the pore volume increased from 97 $\mu L\ g^{-1}$ to 104 (Mt-OH/$Fe_{0.75:1}$) – 116 $\mu L\ g^{-1}$ (Mt-OH/$Fe_{1:1}$) after the modification (Abate and Masini, 2005b). On the other hand, the micropore volume of Mt (1.9 $\mu L\ g^{-1}$) increased significantly in Mt-OH/$Fe_{1:1}$ (5.4 $\mu L\ g^{-1}$) and Mt-OH/$Fe_{2:1}$ (11.7 $\mu L\ g^{-1}$).

FTIR of the K10 Mt and Mt-OH/$Fe_{1:1}$before and after the adsorption of phosphate show that no spectral differences appear after modification of the starting clay mineral, as well as after adsorption of phosphate. All spectra exhibited the typical Al–OH stretching vibrations at 3629 cm^{-1}, the O–H vibrations at 3443 and 1636 cm^{-1} due to adsorbed water, the Si–O stretching vibrations at 1047 cm^{-1}, 698 cm^{-1}, and 475 cm^{-1}, as well as the Si–O–Al–Si vibrations at 526 cm^{-1} (Ren et al., 2014; dos Santos et al., 2015) (Figure 2).

All materials exhibited negative zeta potentials in the pH range between 1 and 11 (Figure 3). The negative charge decreased with the decrease in pH because the surface silanol and aluminol groups became protonated (Avena et al., 1990). Neither the protonation of the surface sites nor the adsorption of the Fe^{3+} polyhydroxy cations compensated for the permanent negative charges at the interlayers. Thus, all the materials were charged negatively at any pH in the studied range. The Mt-OH/$Fe_{0.75:1}$ was the material with less negative zeta potential in acidic medium, consistent with the most significant density of positive charges in this polycation.

3.2. Quantification of Fe^{3+} on the sorbents

The amount of immobilized Fe^{3+} (Table 1) is consistent with the CEC for the K10 Mt (0.59 ± 0.01 mmol g^{-1}), indicating a quantitative exchange of the interlayer cations of the starting mineral by the polyhydroxy cations. The amount of Fe^{3+} was not altered after one adsorption/desorption cycle using a real sample (BR 1) spiked with 80.71 µmol L^{-1} of phosphate or using a pure 1614 µmol L^{-1} phosphate solution. Only a high phosphate concentration (3229 µmol L^{-1}, or 100 mg L^{-1} P) led to measurable decreases of the initially adsorbed Fe^{3+}. In this specific (and somewhat unrealistic) situation, the amount of Fe^{3+} decreased by 9.8% on Mt-OH/$Fe_{2:1}$–14 % in the case of Mt-OH/$Fe_{1:1}$ (Table 1).

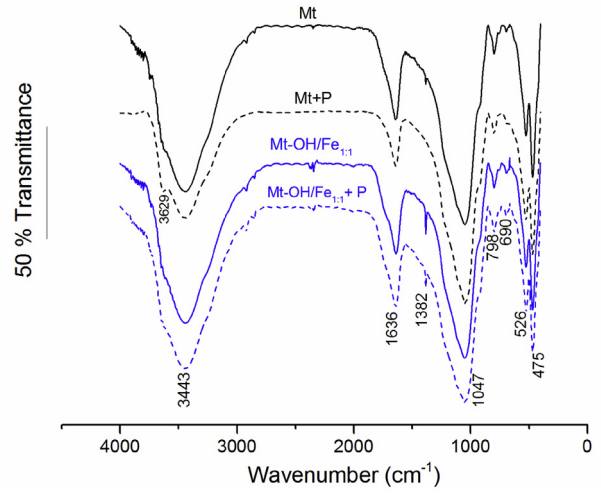

Figure 2. FTIR in KBr of Mt and Mt-OH/$Fe_{1:1}$ in the presence and absence of phosphate.

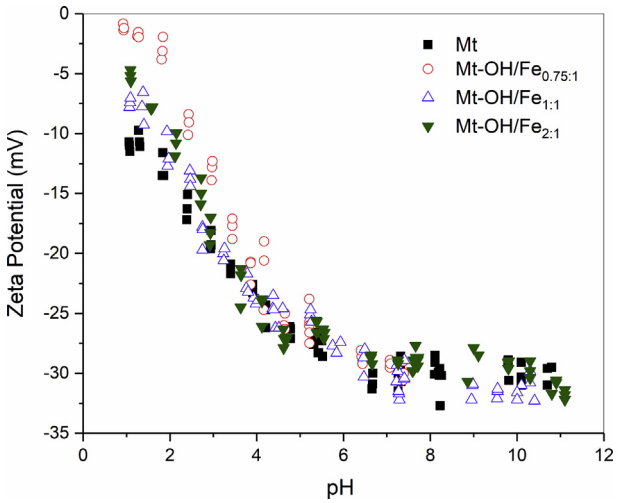

Figure 3. Zeta potential titrations of the K10 Mt compared to the modified materials.

3.3. SEM and EDS

Figure 4 shows the SEM and TEM images of Mt (4A and 4C) and Mt-OH/$Fe_{0.75:1}$ (4B and 4D). The SEM image of Mt-OH/$Fe_{0.75:1}$ is consistent with an increase in the specific surface area compared with that of Mt (Figure 4A). In the EDS analysis, Mt exhibits intense peaks corresponding to the presence of O, Si, and Al (Figure 5a). Other smaller transitions were at the typical transition energies of Cl, Fe, and K, the latter probably behaving as the exchangeable cation (Figure 5a). Residual concentrations of Fe may explain the corresponding transition peaks of this element in the unmodified Mt (Figures 5a and 5b). The incorporation of Fe increased the intensity of these peaks (Figure 6a). However, the surface distribution of Fe was not uniform, denoting the heterogeneity of the studied particles (as suggested by the TEM images in Figure 4). The peak corresponding to the transition energy of P appears in the EDS of the phosphate loaded Mt and Mt-OH/$Fe_{0.75:1}$, exhibiting a higher intensity in Mt-OH/$Fe_{0.75:1}$ than that in the unmodified Mt (Figure 6b).

3.4. Adsorption

3.4.1. Dose/kinetics

The modification of Mt with the Fe^{3+} polyhydroxy cations increased the adsorption capacity of the materials (Figure 7). The increase of the adsorbent dose from 25 to 100 mg improved the adsorption percentages owing to the greater availability of adsorption sites (Funes et al., 2018). On the other hand, the adsorbed amount of phosphate per unit mass of adsorbent (q) systematically decreased because the fixed amount of phosphate was distributed through many more particles of adsorbent (Figure 7) (do Nascimento et al., 2017).

The adsorption was fast in all materials, approaching the equilibrium in approximately 2 h of contact time (Figure 8). The kinetic data obtained with the different doses of adsorbent fitted reasonably to both pseudo 1st and 2nd order models, with the pseudo 2nd order providing better fittings for all materials and doses (Table 2). As the pseudo-2nd order model assumes that a chemical process is a rate-limiting step, the results suggest the chemisorption is the dominant process governing the removal of phosphate (Li et al., 2019). The largest q_e was around 50 µmol g^{-1} (Mt-OH/$Fe_{0.75:1}$ and Mt-OH/$Fe_{1:1}$). Although far from the saturation, this value (about 1.5 mg g^{-1} in P) is lower than those reported in other studies involving bentonites (Borgnino et al., 2009; Zamparas et al., 2012; de Castro et al., 2018). On the other hand, the adsorption was quite fast, reaching a plateau in about 2 h, while other materials required several hours to reach the equilibrium (Lalley et al., 2016; de Castro et al., 2018; Lin et al., 2018).

Table 1. Amount of Fe^{3+} extracted from the adsorbents before any use and after an adsorption/desorption cycle with initial P concentrations of 1614 (P 50), 3229 (P 100), and 80.71 (BR + P 2.50) μmol L^{-1}. Results are the mean of duplicates.

Sorbent	Fe^{3+} extracted (mmol g^{-1})			
	Before use	P 50	P 100	BR + P 2.50
Mt	0.033 ± 0.02	0.030 ± 0.01	0.024 ± 0.01	0.029 ± 0.02
Mt-OH/$Fe_{0.75:1}$	0.54 ± 0.05	0.54 ± 0.02	0.48 ± 0.01	0.57 ± 0.03
Mt-OH/$Fe_{1:1}$	0.57 ± 0.03	0.56 ± 0.03	0.49 ± 0.02	0.54 ± 0.02
Mt-OH/$Fe_{2:1}$	0.63 ± 0.04	0.69 ± 0.05	0.62 ± 0.04	0.64 ± 0.05

Regarding the intraparticle diffusion model, none of the plots of q_t *vs.* $t^{0.5}$ passed through the origin ($C > 0$, Table 2), suggesting that adsorption occurred predominantly on the surface of the modified clay minerals. These results were consistent with the adsorption of phosphate on thermally treated bentonite (Chen et al., 2018), iron oxide-based sorbents (Lalley et al., 2016), zirconium modified bentonite (Lin et al., 2018), and La/Fe modified montmorillonites (de Castro et al., 2018).

3.4.2. Adsorption and desorption isotherms

The Freundlich and Langmuir equations fitted the experimental data of the adsorption isotherms (Figure 9) with $r^2 > 0.90$ (Table 3). The isotherms were of the L-type, meaning that a limited amount of energetically heterogeneous adsorption sites control the adsorption. At low initial concentrations, phosphate occupies the sites with stronger affinity. As these sites are saturated, the adsorption becomes less efficient since the phosphate anions must interact with the sites of lower affinity. Consequently, the adsorption curves tend asymptotically to a constant value of q Figure 9, reaching the saturation, or the q_{max}. The $1/n < 0.44$ (Eq. (7)) reflects the high heterogeneity of the adsorption sites for all the studied materials, even the unmodified Mt, being <0.39 for the materials modified with the Fe^{3+} polyhydroxy cations. The increase of heterogeneity (decrease in 1/n) is consistent with the incorporation of the polyhydroxy cations on the surface of Mt. The K_F values (Eq. (7)) suggest that the adsorption capacities of the modified materials do not differ among them but show a significant increase in comparison with the non-modified Mt.

Fittings with the Langmuir-Freundlich equation were slightly better than those with the Langmuir model (Table 3). The q_{max} order was similar for all the modified montmorillonites, within the experimental error. On the other hand, all the modified materials exhibited larger q_{max} than the unmodified Mt. The K_L values indicate that the strength of interaction does not differ significantly among the modified materials. Still, they are substantially higher than the K_L for the unmodified Mt, reflecting the increased affinity for phosphate.

The adsorption on all the studied materials was predominantly irreversible, as can be observed in the comparison of adsorption and desorption isotherms (Figure 9). The R_L parameter <0.1 (Table 3) also suggests the irreversibility of the adsorption. From the sequential desorption experiments, the hysteresis (Eq. (8)) was <1, confirming the irreversibility of the adsorption. The modification with the Fe^{3+} polyhydroxy cations made the adsorption more irreversible. Thus, while the H value was 0.78 for the unmodified Mt, it was reduced to 0.22–0.26 for the modified materials. The desorption percentages from Mt were around 43.5, 27.0, and 24% in the first, second, and third desorption steps, respectively. Desorption percentages from the modified materials were about 12, 8, and 7% in the respective sequential desorption steps.

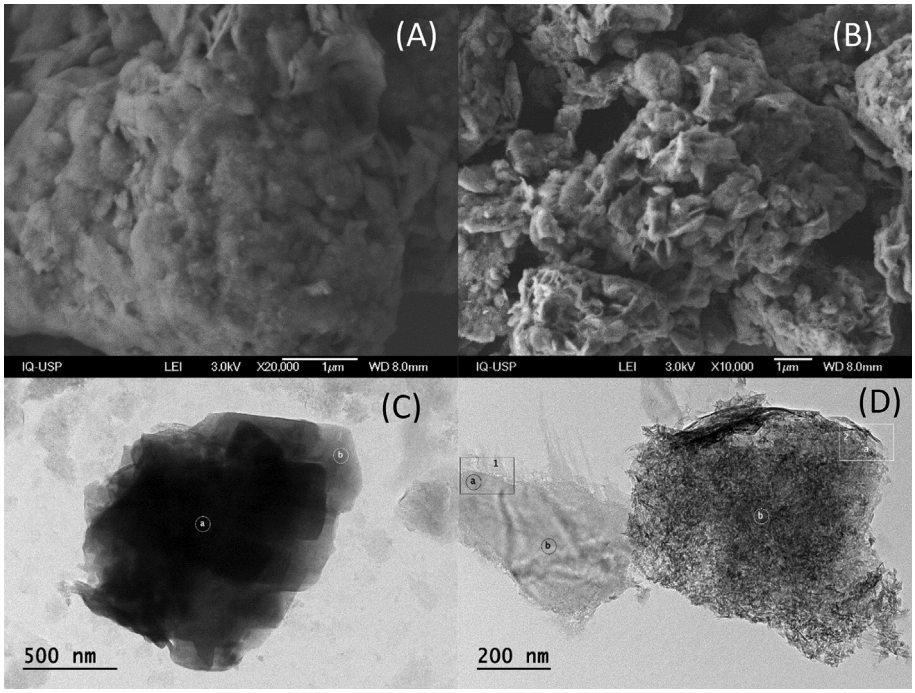

Figure 4. SEM (A and B) and TEM (C and B) images of K10 Mt (A and C) and Mt-OH/$Fe_{2:1}$ (B and D). The spots (1) and (2), (a) and (b) in the TEM images were analyzed by EDS.

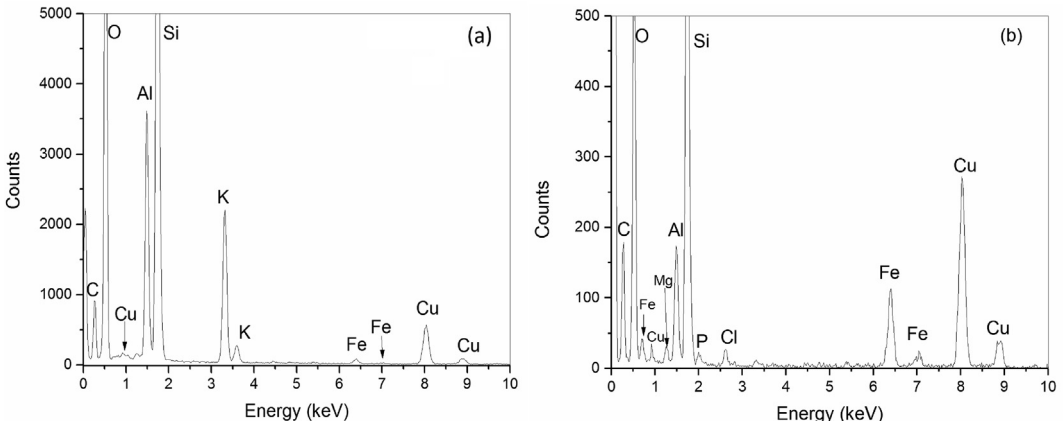

Figure 5. EDS analysis of K10 Mt before phosphate adsorption (a) and loaded with 35 μmol g^{-1} of phosphate (b).

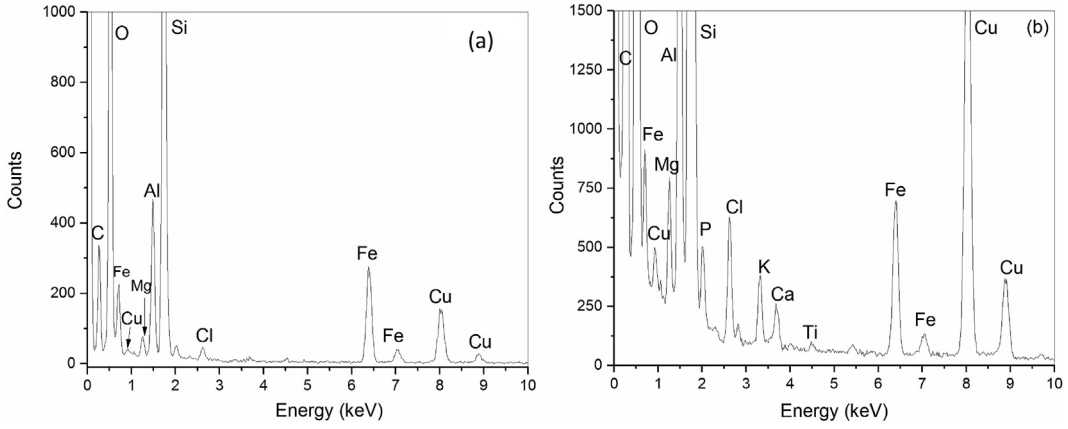

Figure 6. EDS analysis of Mt-OH/$Fe_{0.75:1}$ before phosphate adsorption (a) and loaded with 59 μmol g^{-1} of phosphate (b).

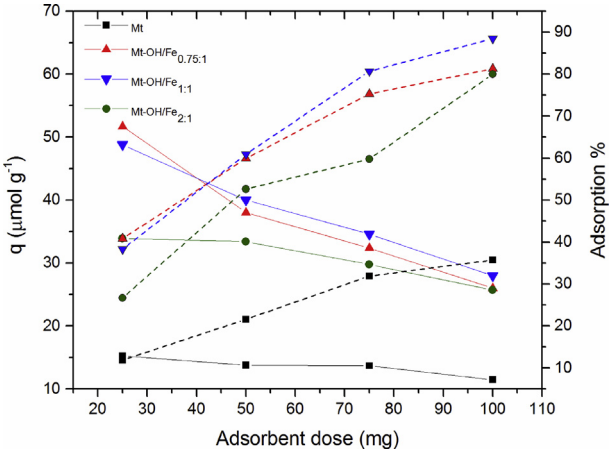

Figure 7. Effect of the dose of adsorbent on the adsorption of phosphate. Experiments made with phosphate initial concentration of 323 μmol L (10 mg L^{-1} in P) at 25.0 ± 0.5 °C, contact time = 180 min, initial pH = 6.90 ± 0.05.

Compared with other adsorbents for phosphate (Table 4), the materials described in the present work exhibited q_{max} of similar magnitude to other K10 montmorillonites modified with La^{3+} and Fe^{3+} (de Castro et al., 2018). They performed better than bentonite thermally treated at 400 °C but performed worse than the same material treated at 800 °C (Chen et al., 2018). The adsorption capacity was predominantly lower than that reported for other adsorbents (Table 4). On the other hand, the surface adsorption was quite fast, and the isotherms were obtained with 3-h of contact time, whereas many other adsorbents required 24 h. Furthermore, the adsorbents prepared here used low-cost materials and environmental-friendly conditions such as near ambient temperature. Preparation of layered Ca, Mg, and La layered chalcogenide, for instance, used the hydrothermal procedure in an autoclave at 200 °C for four days (Li et al., 2019).

Additionally, all the modifications occurred in aqueous solutions, whereas in some cases, solvents such as isopropanol (Huang et al., 2014) and CS_2 (Li et al., 2019) were necessary. Magnetic materials based on hydrous lanthanum oxide loaded silica-coated magnetite are also exciting new adsorbents. Still, their preparation is not as easy as the procedure reported here and involved the use of high-cost organosilane compounds (Funes et al., 2018).

3.5. *Influence of pH and ionic strength*

The adsorption percentages decreased slightly with the increase of pH (Figure 10a). Since the pH of most natural waters lies between 4 and 9, the constancy of the adsorption percentages within this pH range is a useful feature of the proposed adsorbents. Under these conditions, the predominant P species in solution are $H_2PO_4^-$ and HPO_4^{2-}. The commercial Phoslock® exhibited a similar behavior (Zamparas et al., 2015), as well as bentonites modified with either La^{3+} or mixtures of Fe^{3+} and La^{3+} (de Castro et al., 2018). The pH influenced more significantly the adsorption on other materials, showing a systematic decrease in adsorption with the increase of pH (Tian et al., 2009; Huang et al., 2014; Lin et al., 2018). For

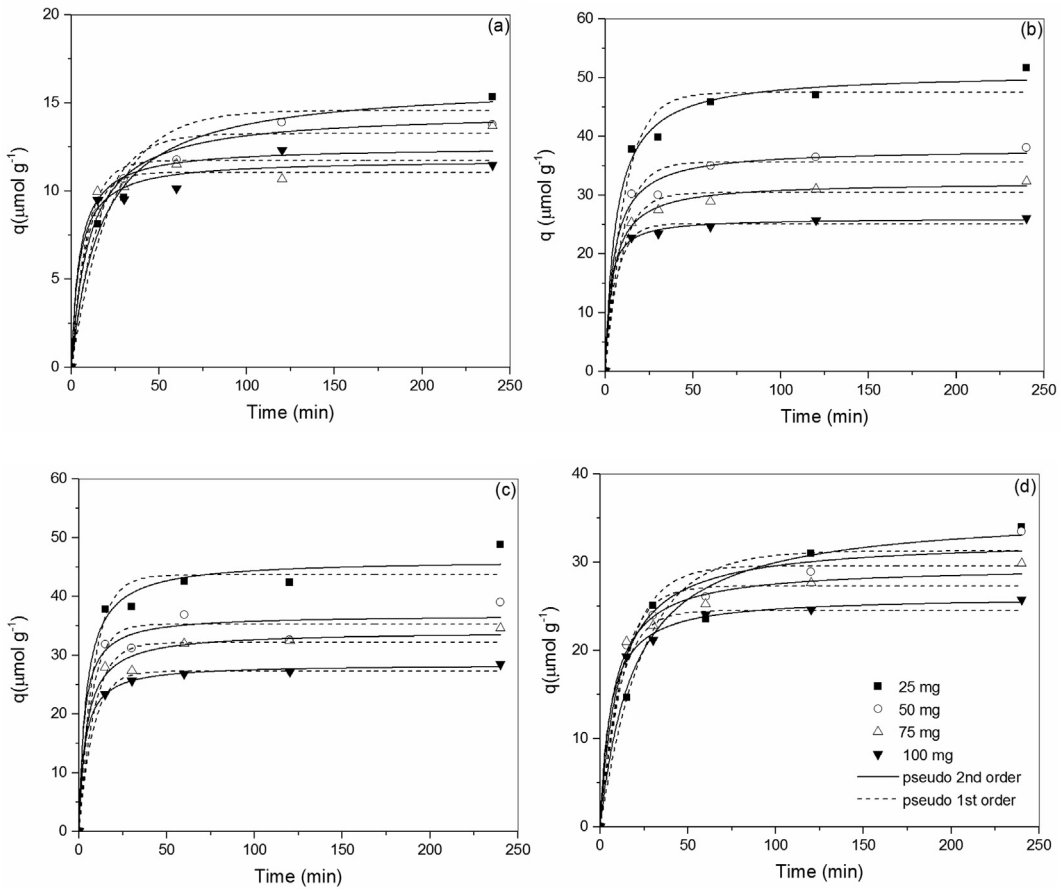

Figure 8. Effect of dose and contact time on the adsorption kinetics of phosphate on (a) Mt, (b) Mt-OH/$Fe_{0.75:1}$, (c) Mt-OH/$Fe_{1:1}$, (d) Mt-OH/$Fe_{2:1}$. Initial concentration of 323 μmol L (10 mg L^{-1} in P) Temperature = 25.0 ± 0.5 °C, initial pH = 6.90 ± 0.05. The experimental data were fitted to the Pseudo 1st order (solid line) and pseudo 2nd order (dashed line) models.

instance, Huang et al. (2014), studying La^{3+} modified exfoliated vermiculite, observed that the adsorption capacity of the material was constant in the pH range between 2 and 7, followed by a sharp decrease in adsorption at pH 8.0, caused by both the increase of negative charges on the adsorbent, and the prevalence of HPO_4^{2-} over $H_2PO_4^-$. Lin et al. (2018) adsorbed phosphate onto bentonites modified with zirconium and observed that the adsorption systematically decreased as the pH increased from 4.0 to 11, accompanied by a systematic increase in the pH of the solution, supporting the hypothesis that hydroxyl groups on the adsorbent are exchanged by phosphate in the adsorption process.

Table 2. Kinetic parameter for adsorption of phosphate at 25.0 ± 0.5 °C from an initial 10 mg L^{-1} P solution (0.323 mmol L^{-1}).

Material	Mass (mg)	Model								
		Pseudo 1st order			Pseudo 2nd order			Intraparticle Diffusion		
		q_e (μmol g^{-1})	k_1 (min^{-1})	R^2	q_e (μmol g^{-1})	$k_2 \times 10^3$ (g μmol^{-1} min^{-1})	R^2	K_{id} (μmol g^{-1} min^{-1})	C (μmol g^{-1})	R^2
Mt	25	14.5 ± 0.7	0.0437 ± 0.007	0.98	16.1 ± 0.6	3.6 ± 0.6	0.994	0.81 ± 0.03	5.1 ± 0.2	0.998
	50	13.2 ± 0.5	0.062 ± 0.01	0.98	14.5 ± 0.4	7 ± 1	0.994	0.69 ± 0.08	6.5 ± 0.5	0.97
	75	11.7 ± 0.7	0.11 ± 0.04	0.94	12.4 ± 0.8	17 ± 8	0.96	0.12 ± 0.12	9.7 ± 0.9	0.31
	100	11.1 ± 0.1	0.11 ± 0 04	0.95	11.7 ± 0.5	19 ± 9	0.98	0.4 ± 0.1	7.5 ± 0.8	0.88
Mt-OH/$Fe_{0.75:1}$	25	47 ± 2	0.091 ± 0.02	0.97	51 ± 2	3.2 ± 0.8	0.991	1.4 ± 0.3	32 ± 3	0.89
	50	36 ± 1	0.11 ± 0.03	0.97	38 ± 1	6 ± 1	0.990	1.0 ± 0.2	26 ± 2	0.87
	75	30.4 ± 0.2	0.11 ± 0.02	0.98	32.1 ± 0.5	7 ± 1	0.997	0.77 ± 0.09	22.7 ± 0.7	0.97
	100	25.1 ± 0.5	0.15 ± 0.03	0.86	26.0 ± 0.3	15 ± 3	0.998	0.42 ± 0.03	21.1 ± 0.2	0.99
Mt-OH/$Fe_{1:1}$	25	44 ± 2	0.11 ± 0.04	0.96	46 ± 2	5 ± 1	0.98	0.75 ± 0.10	35 ± 1	0.94
	50	35 ± 2	0.14 ± 0.05	0.96	37 ± 2	9 ± 1	0.97	0.45 ± 0.21	30 ± 2	0.59
	75	22 ± 1	0.12 ± 0.03	0.97	34 ± 1	7 ± 2	0.98	0.48 ± 0.13	23 ± 2	0.81
	100	27.2 ± 0.4	0.12 ± 0.01	0.99	28.3 ± 0.2	10 ± 1	0.999	0.29 ± 0.09	24 ± 1	
Mt-OH/$Fe_{2:1}$	25	31 ± 2	0.04 ± 0.01	0.94	35 ± 3	1.4 ± 0.5	0.967	2.31 ± 0.01	5.7 ± 0.1	0.999
	50	30 ± 1	0.07 ± 0.01	0.95	33 ± 1	3.0 ± 0.8	0.98	1.1 ± 0.2	17 ± 1	0.96
	75	27 ± 1	0.08 ± 0.01	0.97	29.4 ± 0.9	4.7 ± 0.9	0.99	0.94 ± 0.06	17.6 ± 0.5	0.99
	100	24.5 ± 0.7	0.09 ± 0.01	0.98	26.0 ± 0.4	6.7 ± 0.8	0.99	0.76 ± 0.20	17 ± 2	0.87

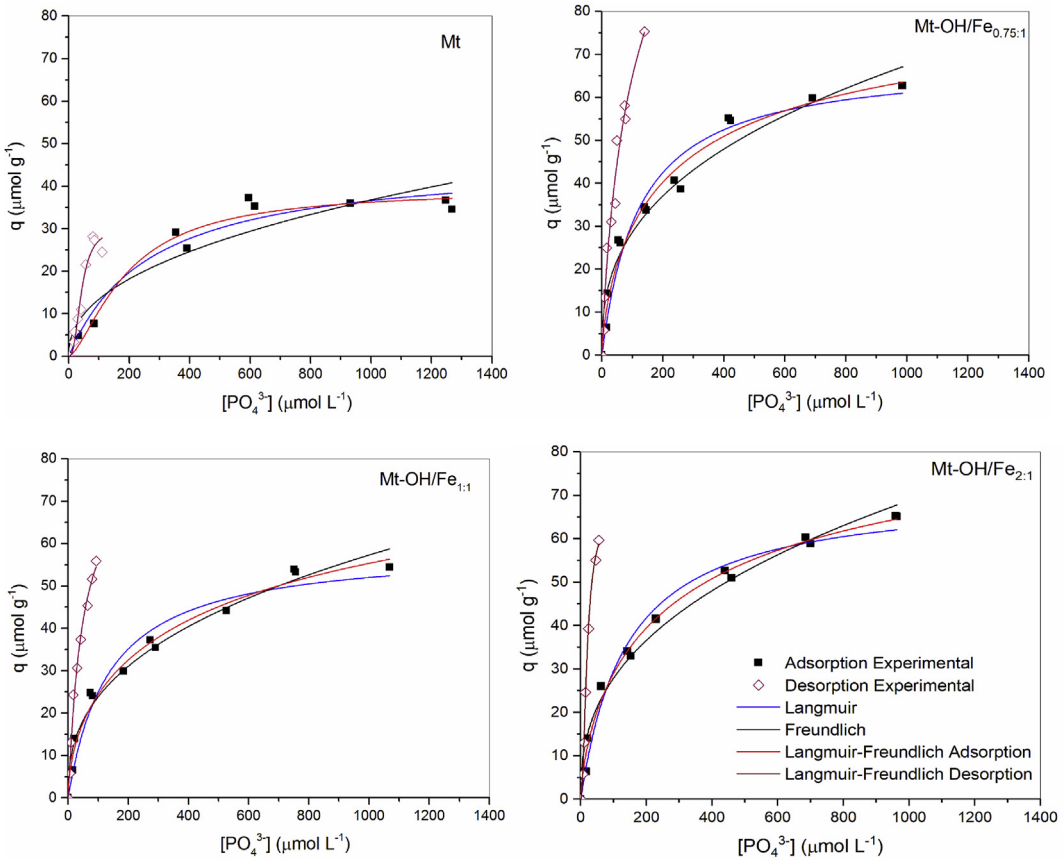

Figure 9. Adsorption and desorption isotherms at 25.0 ± 0.5 °C using a mass of 100 ± 2 mg of adsorbent and initial phosphate concentrations varying from 10 to 100 mg L^{-1} (in P), that is, between 323 and 3,230 μmol L^{-1} in phosphate. Contact time = 180 min.

Table 3. Adsorption and desorption parameters obtained from Langmuir and Freundlich isotherms.

Process	Model	Parameter	Material			
			Mt	Mt-OH/$Fe_{0.75:1}$	Mt-OH/$Fe_{1:1}$	Mt-OH/$Fe_{2:1}$
Adsorption	Langmuir	q_{max} (μmol g^{-1})	46 ± 3	68 ± 3	59 ± 3	71 ± 3
		K_L (L μmol^{-1})	(3.7 ± 0.9) × 10^{-3}	(8 ± 1) × 10^{-3}	(7 ± 1) × 10^{-3}	(7.1 ± 0.9) × 10^{-3}
		R^2	0.96	0.96	0.95	0.98
		R_L	0.0772	0.0373	0.0424	0.0418
	Freundlich	1/n	0.44 ± 0.07	0.37 ± 0.03	0.38 ± 0.02	0.39 ± 0.02
		K_F ($\mu mol^{1-1/n}$ g^{-1} $L^{1/n}$)	1.8 ± 0.9	5.1 ± 0.9	4.1 ± 0.6	4.6 ± 0.6
		R^2	0.88	0.95	0.97	0.98
	Langmuir-Freundlich	q_{max} (μmol g^{-1})	39 ± 2	88 ± 15	104 ± 15	95 ± 12
		K_{LF} (L μmol^{-1})	(3 ± 4) × 10^{-4}	0.020 ± 0.006	0.022 ± 0.004	0.018 ± 0.004
		n_2	-0.59 ± 0.26	0.29 ± 0.11	0.43 ± 0.10	0.31 ± 0.08
		R^2	0.97	0.97	0.98	0.99
Desorption	Langmuir-Freundlich	q_{max} (μmol g^{-1})	30 ± 4	140 ± 71	80 ± 21	66 ± 3
		K_{LF} (L μmol^{-1})	(6.4 ± 0.2) × 10^{-5}	0.016 ± 0.006	0.017 ± 0.007	0.003 ± 0.001
		n_2	-1.6 ± 0.9	0.1 ± 0.2	0.0 ± 0.2	-1.0 ± 0.2
		R^2	0.94	0.97	0.98	0.997
Sequential Desorption	Freundlich	$1/n_d$	0.34	0.096	0.0951	0.0874
		H	0.78	0.26	0.25	0.22
		R^2	0.98	0.97	0.98	0.99

In the present study, the K10 Mt caused a significant reduction of the solution pH after the contact time of 180 min. The pH of the initial phosphate solution dropped from 6.9 to about 4–5, depending on the initial phosphate concentration (Figure 11). Similar behavior was observed for the modified materials, which also acidified the medium, probably by hydrolysis of the Fe^{3+} hydroxyl ions. Mixing aragonite with the adsorbent at a 1:1 mass ratio neutralized the medium without affecting the adsorption percentages (Table 5).

In the absence of aragonite, after the initial abrupt drop, the pH systematically increased with the initial phosphate concentration as the

Table 4. Other Materials. Data relative to adsorption isotherms constructed at 298 K and fitted by the Langmuir isotherm.

Adsorbent	q_{max} [a] (μmol g^{-1})	pH	P range (μmol L^{-1})	Contact time (h)	Dose (g L^{-1})	Reference
Phoslock™	122	7.0	1.6–160	3	0.40	Zamparas et al. (2012)
Fe/Zenith bentonite	360	7.0	0.0526–52.6	3	0.40	Zamparas et al. (2012)
Al/Fe or Fe/Al - bentonite	181–364	5.0	105–526	9	2.0	Shanableh et al. (2016)
La/Al Mt	332–420	5.0	80.7–1614	12	2.5	Tian et al. (2009)
La/Fe Mt	30.1–188	6.0	5.2–42455	96	5.0	de Castro et al. (2018)
Acid activated akadama clay	101	6.9	105–1053	24	5.0	Wang et al. (2018)
La, Ca, Mg layered chalcogenide	387–635	6.5	Not informed	24	1.0	Li et al. (2019)
Thermally treated bentonite	15.5 (400 °C) 224 (800 °C)	7.0	7.35–2206	24	20	Chen et al. (2018)
Zirconium bentonite	292.5–432.6	7.0	64.6–1130	24	1.0	Lin et al. (2018)
Zr/Al pillared Mt	555	5.0	645–1614	24	2.0	Huang et al. (2015)
$La(OH)_3$ exfoliated vermiculite	2.57×10^3	5.0	32.2–3220	48	1.0	Huang et al. (2014)
g-C_3N_4/Mt	53.2	6.0	52.6–684	2	1.0	(Wan et al., 2019)

[a] For comparison purpose all the adsorption capacities were converted to μmol g^{-1}.

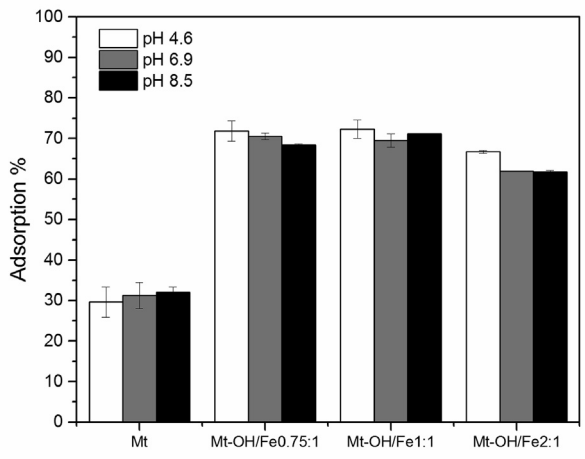

Figure 10. Influence of the initial pH on the adsorption of phosphate from a 484 μmol L^{-1} solution (15 mg L^{-1} in P) using 100 mg of adsorbent dispersed in 10.0 mL of solution and 180 min of contact time at 25.0 ± 0.5 °C.

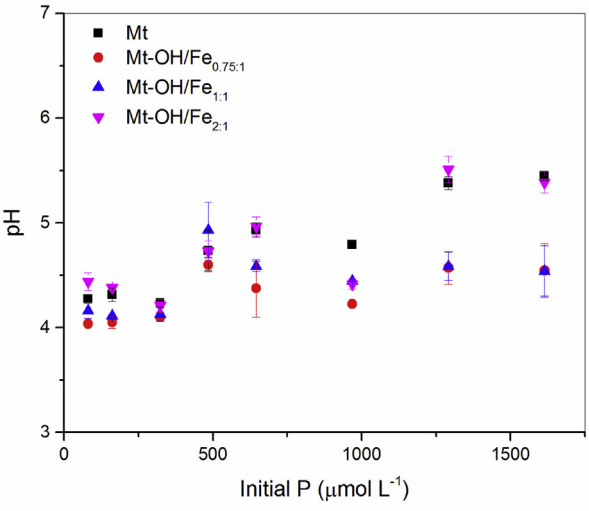

Figure 11. Solution pH at the contact time of 180 min used for the construction of the adsorption isotherms (25.0 ± 0.5 °C) using 100 ± 2 mg of adsorbent dispersed in 10.0 mL of solution. Initial pH = 6.90.

system reached the equilibrium (Figure 11). This release of small amounts of OH^- coinciding with the adsorption of phosphate is consistent with the ligand exchange mechanism. Huang et al. (2014) attributed to the ligand exchange mechanism the increase in the pH from 5.47 to 10.23 as the adsorption on $La(OH)_3$-modified exfoliated vermiculites proceeded along 12 h.

Adsorption percentages increased systematically with the ionic strength (Figure 12). Since the adsorbents were negative at any range of pH (Figure 3), the increase in ionic strength may have shielded these negative charges, thus minimizing electrostatic repulsion between phosphate anions and the surface of the adsorbents. The enhanced adsorption at higher ionic strength supports the hypothesis of the formation of inner-sphere complexes between phosphate and the Fe^{3+} polyhydroxy cations on the surface of the particles.

3.6. Effect of coexisting compounds

Adsorption experiments were made using 50.0 mg of adsorbent dispersed in 5.0 mL of 80.7 μmol L^{-1} phosphate buffer (pH 6.90) (2.5 mg L^{-1} in P) in the absence (control) and presence of humic acid (10.0 mg L^{-1}), fulvic acid (10.0 mg L^{-1}), $NaNO_3$ (10.0 mg L^{-1}), $NaNO_2$ (1.0 mg L^{-1}) and NH_4Cl (10.0 mg L^{-1}). Compared to the control experiment, the coexisting compounds did not decrease the adsorption percentages (Figure 13). The influence of salts may be similar to that observed for the effect of ionic strength, that is, the increased salt concentration may have shielded the negative charges of the adsorbents, favoring the formation of inner-sphere complexes between phosphate and the Fe^{3+} polycations. Humic and fulvic acids, the predominant natural organic matter components in aquatic environments, also have significant amounts of Fe^{3+} and other di- or trivalent cations that may have favored the adsorption of phosphate by the formation of surface complexes. Zirconium-modified bentonites exhibited similar behavior, as demonstrated by Lin et al. (2018). On the contrary, Zr/Al modified montmorillonites exhibited a small decrease in adsorbed phosphate in the presence anions such as NO_3^-, Cl^-, SO_4^{2-} and CO_3^{2-} (Huang et al., 2015). That is, there is no clear trend in the effect of coexisting species comparing the proposed materials with others recently described.

3.7. Reusability

Since the desorption in water was not higher than 12%, we investigated the effect of a sequence of three cycles of adsorption, intercalated by washing with deionized water, observing a systematic decrease in the adsorption percentages (Figure 14) caused by the residual adsorbed phosphate. After two adsorption cycles with adsorption percentages >70%, in the third adsorption cycle, the adsorption decreased to about 36%. It is interesting to note that the Fe^{3+} modified material performed

Table 5. Effect of mixing aragonite (Arag) with K10 Mt and modified Mt on the pH and adsorption percentage from an 80.7 μmol L^{-1} phosphate solution. Experimental conditions: mass of aragonite = mass of adsorbent = 50.0 ± 0.5 mg. Stirring rate = 250 r.p.m., contact time = 180 min, temperature = 25.0 ± 0.5 °C. Results are the mean of two experiments.

Material	Adsorption %	Initial pH	Final pH
Mt	62 ± 1	6.90 ± 0.01	4.28 ± 0.04
Mt-OH/$Fe_{0.75:1}$	80 ± 2	6.90 ± 0.01	4.04 ± 0.01
Mt-OH/$Fe_{1:1}$	80 ± 2	6.90 ± 0.01	4.16 ± 0.07
Mt-OH/$Fe_{2:1}$	74 ± 3	6.90 ± 0.01	4.44 ± 0.08
Mt + Arag	40 ± 4	6.76 ± 0.12	7.67 ± 0.06
Mt-OH/$Fe_{0.75:1}$ + Arag	74.2 ± 0.4	6.41 ± 0.01	7.77 ± 0.01
Mt-OH/$Fe_{1:1}$ + Arag	78 ± 2	6.57 ± 0.17	7.75 ± 0.10
Mt-OH/$Fe_{2:1}$ + Arag	76 ± 4	6.15 ± 0.10	7.65 ± 0.06
Arag	-	9.10 ± 0.10	8.60 ± 0.10

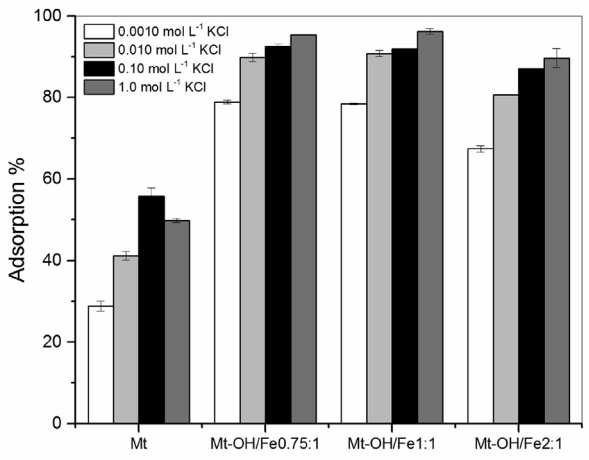

Figure 12. Influence of the ionic strength (at pH 6.90) on the adsorption of phosphate from a 484 μmol L^{-1} solution (15 mg L^{-1} in P) using 100 mg of adsorbent dispersed in 10.0 mL of solution and 180 min of contact time.

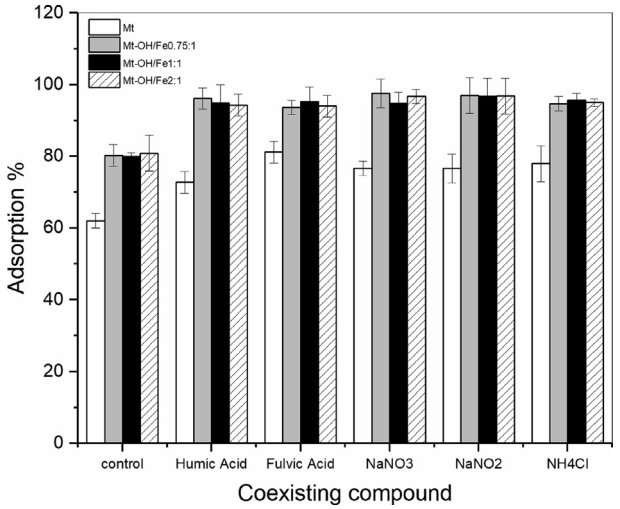

Figure 13. Effect of coexisting substances on the adsorption from an 80.7 μmol L^{-1} phosphate solution (2.5 mg L^{-1} in P). Dose = 50 mg, volume = 5.0 mL, pH 6.90, contact time = 180 min, temperature = 25.0 ± 0.5 °C.

much better than the unmodified K10 Mt, which did not adsorb phosphate in the third adsorption cycle. It is usual in this kind of study to perform a regenerating cycle with 0.10 mol L^{-1} NaOH between the adsorption cycles (Tian et al., 2009; Huang et al., 2014). In the present study, this treatment dissolved part of the silica, thus causing a drastic decrease in the desorption capacity.

3.8. Application to real samples

The dissolved phosphate concentrations (as P) found in the studied samples were 0.0971, 0.0919, and 1.211 mg L^{-1} for BR1, BR2, and PR1, respectively. All samples exceed the maximum concentration level of 0.075 mg L^{-1} recommended by the Brazilian National Environment Council (CONAMA) for class 3 freshwaters, which require conventional or advanced treatment for human consumption. Adsorption made directly in the water samples resulted in quantitative adsorption, that is, the residual concentration of phosphate was less than the limit of quantification of the analytical method (0.063 mg L^{-1} in P, or 2.0 μmol L^{-1}). Samples spiked with 2.58–3.59 mg L^{-1} in P (83.1–116 μmol L^{-1}) exhibited adsorption percentages between 89.4 and 94.8% (Table 6). Although the residual concentration exceeded the maximum level allowed by CONAMA (0.075 mg L^{-1}), the real matrix of three polluted water did not block the adsorption sites. Even the unmodified Mt adsorbed 74–85% of the initial phosphate in the real samples.

4. Conclusions

The modification of the K10 Mt with Fe^{3+} polyhydroxy cations enhanced the capacity and affinity of the resulting materials for phosphate adsorption. The maximum adsorption capacities (q_{max}) of the modified materials were roughly 125–156% higher than that of the unmodified Mt. Phosphate was firmly bound to the adsorbent, exhibiting

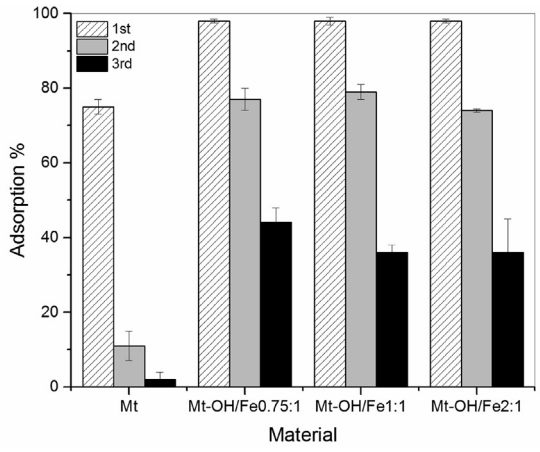

Figure 14. Adsorption percentages in three sequential steps of adsorption using initial phosphate concentration of 80.7 μmol L^{-1} (2.50 mg L^{-1} in P). Experimental conditions: contact times = 180 min, temperature = 25.0 ± 0.5 °C, stirring rate = 250 r.p.m.

Table 6. Adsorption percentages found in adsorption experiments made different water samples. Experimental conditions: 100 mg adsorbent to 5.0 mL sample, 180 min contact time, 25.0 ± 0.5 °C, stirring rate = 180 r.p.m.

Sample	Initial P Conc. (μmol L^{-1})	Adsorption %			
		Mt	Mt-OH/$Fe_{0.75:1}$	Mt-OH/$Fe_{1:1}$	Mt-OH/$Fe_{2:1}$
D.I. Water	80.7	62 ± 3	80.3 ± 0.5	80.0 ± 0.8	80.9 ± 0.3
BR1	81.3	85.3 ± 0.1	90.8 ± 0.1	94.8 ± 0.3	94.1 ± 0.2
BR2	83.3	77 ± 2	94.3 ± 0.3	93.2 ± 0.2	94 ± 1
PR1	115.9	74 ± 2	91.1 ± 0.8	90.6 ± 0.3	89.4 ± 0.1

irreversible interaction. Although the adsorption capacity of the proposed materials is lower than several other adsorbents, the adsorption is quite fast, and the modification is simple, using low cost-environmentally compatible Fe^{3+} salts. The prepared adsorbents were efficient in removing phosphate from three polluted aquatic samples. Future work will evaluate the described adsorbents for the removal of other oxyanions (arsenate, chromate, etc).

Declarations

Author contribution statement

Jorge Masini: Conceived and designed the experiments; Analyzed and interpreted the data; Contributed reagents, materials, analysis tools or data; Wrote the paper.

Samara T. Leite: Performed the experiments; Analyzed and interpreted the data; Contributed reagents, materials, analysis tools or data.

Fernando H. do Nascimento: Analyzed and interpreted the data; Wrote the paper.

Funding statement

Jorge Masini was supported by Conselho Nacional de Desenvolvimento Científico e Tecnológico (303940/2017-4). Samara T. Leite was supported by Conselho Nacional de Desenvolvimento Científico e Tecnológico (141106/2016-6). Fernando H. do Nascimento was supported by Coordenação de Aperfeiçoamento de Pessoal de Nível Superior (88882.315696/2019-01).

Competing interest statement

The authors declare no conflict of interest.

Additional information

No additional information is available for this paper.

Acknowledgements

We recognize the São Paulo State Environmental Company (CETESB) for providing relevant water samples contaminated with phosphate.

References

Abate, G., dos Santos, L.B.O., Colombo, S.M., Masini, J.C., 2006. Removal of fulvic acid from aqueous media by adsorption onto modified vermiculite. Appl. Clay Sci. 32, 261–270.

Abate, G., Masini, J.C., 2005a. Sorption of atrazine, propazine, deethylatrazine, deisopropylatrazine and hydroxyatrazine onto organovermiculite. J. Braz. Chem. Soc. 16, 936–943.

Abate, G., Masini, J.C., 2005b. Adsorption of atrazine, hydroxyatrazine, deethylatrazine, and deisopropylatrazine onto Fe(III) polyhydroxy cations intercalated vermiculite and montmorillonite. J. Agric. Food Chem. 53, 1612–1619.

Adewuyi, A., Oderinde, R.A., 2019. Chemically modified vermiculite clay: a means to remove emerging contaminant from polluted water system in developing nation. Polym. Bull. 76, 4967–4989.

Almasri, D.A., Rhadfi, T., Atieh, M.A., McKay, G., Ahzi, S., 2018. High performance hydroxyiron modified montmorillonite nanoclay adsorbent for arsenite removal. Chem. Eng. J. 335, 1–12.

Avena, M.J., Cabrol, R., De Pauli, C.P., 1990. Study of some physicochemical properties of pillared montmorillonites: acid-base potentiometric titrations and electrophoretic measurements. Clays Clay Miner 38, 356–362.

Borgnino, L., Avena, M.J., De Pauli, C.P., 2009. Synthesis and characterization of Fe(III)-montmorillonites for phosphate adsorption. Colloids Surfaces A Physicochem. Eng. Asp. 341, 46–52.

Chen, X., Wu, L., Liu, F., Luo, P., Zhuang, X., Wu, J., Zhu, Z., Xu, S., Xie, G., 2018. Performance and mechanisms of thermally treated bentonite for enhanced phosphate removal from wastewater. Environ. Sci. Pollut. Res. 25, 15980–15989.

Cunha, D.G.F., Casali, S.P., de Falco, P.B., Thornhill, I., Loiselle, S.A., 2017. The contribution of volunteer-based monitoring data to the assessment of harmful phytoplankton blooms in Brazilian urban streams. Sci. Total Environ. 584–585, 586–594.

de Castro, L., Brandão, V., Bertolino, L., de Souza, W., Teixeira, V., 2018. Phosphate adsorption by montmorillonites modified with lanthanum/iron and a laboratory test using water from the Jacarepaguá lagoon (RJ, Brazil). J. Braz. Chem. Soc. 30, 641–657.

do Nascimento, F.H., de Souza Costa, D.M., Masini, J.C., 2016. Evaluation of thiol-modified vermiculite for removal of Hg(II) from aqueous solutions. Appl. Clay Sci. 124–125, 227–235.

do Nascimento, F.H., Rigobello-Masini, M., Domingos, R.F., Pinheiro, J.P., Masini, J.C., 2017. Dynamic interactions of Hg(II) with the surface of green microalgae Chlamydomonas reinhardtii studied by stripping chronopotentiometry. Algal Res. 24, 347–353.

dos Anjos, V.E., Rohwedder, J.R., Cadore, S., Abate, G., Grassi, M.T., 2014. Montmorillonite and vermiculite as solid phases for the preconcentration of trace elements in natural waters: adsorption and desorption studies of As, Ba, Cu, Cd, Co, Cr, Mn, Ni, Pb, Sr, V, and Zn. Appl. Clay Sci. 99, 289–296.

dos Santos, V.C.G., Grassi, M.T., Abate, G., 2015. Sorption of Hg(II) by modified K10 montmorillonite: influence of pH, ionic strength and the treatment with different cations. Geoderma 237, 129–136.

Fang, L., Liu, R., Li, J., Xu, C., Huang, L.Z., Wang, D., 2018. Magnetite/Lanthanum hydroxide for phosphate sequestration and recovery from lake and the attenuation effects of sediment particles. Water Res. 130, 243–254.

Funes, A., Martínez, F.J., Álvarez-Manzaneda, I., Conde-Porcuna, J.M., de Vicente, J., Guerrero, F., de Vicente, I., 2018. Determining major factors controlling phosphorus removal by promising adsorbents used for lake restoration: a linear mixed model approach. Water Res. 141, 377–386.

Galhardo, C.X., Masini, J.C., 2000. Spectrophotometric determination of phosphate and silicate by sequential injection using molybdenum blue chemistry. Anal. Chim. Acta 417, 191–200.

Hall, K.R., Eagleton, L.C., Acrivos, A., Vermeulen, T., 1966. Pore- and solid-diffusion kinetics in fixed-bed adsorption under constant-pattern conditions. Ind. Eng. Chem. Fund. 5, 212–223.

Huang, W., Chen, J., He, F., Tang, J., Li, D., Zhu, Y., Zhang, Y., 2015. Effective phosphate adsorption by Zr/Al-pillared montmorillonite: insight into equilibrium, kinetics and thermodynamics. Appl. Clay Sci. 104, 252–260.

Huang, W.Y., Li, D., Liu, Z.Q., Tao, Q., Zhu, Y., Yang, J., Zhang, Y.M., 2014. Kinetics, isotherm, thermodynamic, and adsorption mechanism studies of La(OH)3-modified exfoliated vermiculites as highly efficient phosphate adsorbents. Chem. Eng. J. 236, 191–201.

Ivanets, A., Kitikova, N., Shashkova, I., Matrunchik, Y., Kul'bitskaya, L., Sillanpää, M., 2016. Non-acidic synthesis of phosphatized dolomite and its sorption behaviour towards Pb 2+, Zn2+, Cu2+, Cd2+, Ni2+, Sr2+ and Co2+ ions in multicomponent aqueous solution. Environ. Technol. Innov. 6, 152–164.

Ivanets, A.I., Shashkova, I.L., Kitikova, N.V., Kul'Bitskaya, L.V., Matrunchik, Y.V., 2015. Study of the interaction of mono-, di-, and trisubstituted sodium orthophosphates with thermally activated dolomite. Russ. J. Appl. Chem. 88, 1757–1762.

Kasprzyk, M., Gajewska, M., 2019. Phosphorus removal by application of natural and semi-natural materials for possible recovery according to assumptions of circular economy and closed circuit of P. Sci. Total Environ. 650, 249–256.

Koh, K.Y., Zhang, S., Paul Chen, J., 2020. Hydrothermally synthesized lanthanum carbonate nanorod for adsorption of phosphorus: material synthesis and optimization, and demonstration of excellent performance. Chem. Eng. J. 380, 122153.

Kong, L., Tian, Y., Li, N., Liu, Y., Zhang, Jian, Zhang, Jun, Zuo, W., 2018. Highly-effective phosphate removal from aqueous solutions by calcined nano-porous palygorskite matrix with embedded lanthanum hydroxide. Appl. Clay Sci. 162, 507–517.

Kuźniarska-Biernacka, I., Pereira, C., Carvalho, A.P., Pires, J., Freire, C., 2009. K10-montmorillonite as support for a cationic manganese(III)-salen complex. J. Braz. Chem. Soc. 20, 1320–1326.

Lalley, J., Han, C., Li, X., Dionysiou, D.D., Nadagouda, M.N., 2016. Phosphate adsorption using modified iron oxide-based sorbents in lake water: kinetics, equilibrium, and column tests. Chem. Eng. J. 284, 1386–1396.

Li, J.R., Wang, F.K., Xiao, H., Xu, L., Fu, M.L., 2019. Layered chalcogenide modified by Lanthanum, calcium and magnesium for the removal of phosphate from water. Colloids Surfaces A Physicochem. Eng. Asp. 560, 306–314.

Lin, J., He, S., Zhan, Y., Zhang, H., 2020. Evaluation of phosphate adsorption on zirconium/magnesium-modified bentonite. Environ. Technol. (United Kingdom) 41, 586–602.

Lin, J., Jiang, B., Zhan, Y., 2018. Effect of pre-treatment of bentonite with sodium and calcium ions on phosphate adsorption onto zirconium-modified bentonite. J. Environ. Manag. 217, 183–195.

Mdlalose, L., Balogun, M., Setshedi, K., Chimuka, L., Chetty, A., 2019. Adsorption of phosphates using transition metals-modified bentonite clay. Separ. Sci. Technol. 54, 2397–2408.

Ren, X., Zhang, Z., Luo, H., Hu, B., Dang, Z., Yang, C., Li, L., 2014. Adsorption of arsenic on modified montmorillonite. Appl. Clay Sci. 97–98, 17–23.

Savic, I.M., Stojiljkovic, S.T., Savic, I.M., Stojanovic, S.B., Moder, K., 2012. Modeling and optimization of fe(III) adsorption from water using bentonite clay: comparison of central composite design and artificial neural network. Chem. Eng. Technol. 35, 2007–2014.

Shanableh, A., Enshasi, G., Elsergany, M., 2016. Phosphorous adsorption using Al3+/Fe3+-modified bentonite adsorbents—effect of Al3+ and Fe3+ combinations. Desalination Water Treat. 57, 15628–15634.

Tian, S., Jiang, P., Ning, P., Su, Y., 2009. Enhanced adsorption removal of phosphate from water by mixed lanthanum/aluminum pillared montmorillonite. Chem. Eng. J. 151, 141–148.

Uddin, M.K., 2017. A review on the adsorption of heavy metals by clay minerals, with special focus on the past decade. Chem. Eng. J. 308, 438–462.

Wallis, P.J., Gates, W.P., Patti, A.F., Scott, L., Teoh, E., 2007. Cutting-edge research for a greener sustainable future Assessing and improving the catalytic activity of K-10 montmorillonite. Green Chem. 9, 980–985.

Wan, X., Khan, M.A., Wang, F., Xia, M., Lei, W., Zhu, S., Fu, C., Ding, Y., 2019. Facile synthesis of protonated g-C3N4 and acid-activated montmorillonite composite with efficient adsorption capacity for PO43− and Pb(II). Chem. Eng. Res. Des. 152, 95–105.

Wang, Y., He, H., Zhang, N., Shimizu, K., Lei, Z., Zhang, Z., 2018. Efficient capture of phosphate from aqueous solution using acid activated akadama clay and mechanisms analysis. Water Sci. Technol. 78, 1603–1614.

Yan, L.G., Xu, Y.Y., Yu, H.Q., Xin, X.D., Wei, Q., Du, B., 2010. Adsorption of phosphate from aqueous solution by hydroxy-aluminum, hydroxy-iron and hydroxy-iron-aluminum pillared bentonites. J. Hazard Mater. 179, 244–250.

Yang, S., Ren, X., Zhao, G., Shi, W., Montavon, G., Grambow, B., Wang, X., 2015. Competitive sorption and selective sequence of Cu (II) and Ni (II) on ScienceDirect Competitive sorption and selective sequence of Cu (II) and Ni (II) on montmorillonite : batch , modeling , EPR and XAS studies. Geochim. Cosmochim. Acta 166, 129–145.

Zamparas, M., Gavriil, G., Coutelieris, F.A., Zacharias, I., 2015. A theoretical and experimental study on the P-adsorption capacity of Phoslock™. Appl. Surf. Sci. 335, 147–152.

Zamparas, M., Gianni, A., Stathi, P., Deligiannakis, Y., Zacharias, I., 2012. Removal of phosphate from natural waters using innovative modified bentonites. Appl. Clay Sci. 62–63, 101–106.